ELSEVIER

Materials Science and Engineering B42 (1996) 172–175

MATERIALS SCIENCE & ENGINEERING B

SCH laser recombination rate from EBIC profiles

M.J. Romero*, D. Araújo, R. García

Departamento de Ciencia de los Materiales e I.M. y Q.I., Facultad de Ciencias, Universidad de Cádiz. Apdo. 40, 11510 Puerto Real (Cádiz), Spain

Abstract

A new method to evaluate the total recombination velocity R at the quantum wells (QW) using electron-beam-induced current (EBIC) linescans is presented. The procedure consists in, as a first step, estimating the electron–hole pairs (e–h) generation function $g(x, y, z)$ applying Monte Carlo calculations where the incident electron energy dependence of the inelastic–elastic scattering cross-section proportion is introduced. Secondly, the steady-state diffusion equation is applied to minority carriers in each differential volume of e–h generation. This method is then used to investigate separate-confinement laser heterostructures (SCH). From the comparison between experimental and calculated EBIC linescans, minority carriers diffusion lengths at both sides of the laser junction and recombination rate in the active region are deduced. As a result, the recombination rate in the QWs of the laser structure is evaluated to be $R \approx 3 \times 10^6$ cm s^{-1}.

Keywords: Electron-beam-induced current; Electron–hole pairs; Separate-confinement laser heterostructures

1. Introduction

The electron-beam-induced current (EBIC) and cathodoluminescence (CL) modes of scanning electron microscopy (SEM) are powerful techniques for the investigation of semiconductors and are based on opto- and microelectronic devices [1,2]. Nevertheless, quantitative analysis of these modes did not deliver up to now all the possible information available. This is due mainly to the extent of electron-hole pairs (e–h) generation during electron beam excitation that complicates the interpretation of CL and/or EBIC measurements. To overcome these difficulties, the e–h generation spatial dependence is estimated and taken into account in the EBIC intensity profile simulation. The distributions of generated e–h are determined through Monte Carlo calculations applied to the s-scattering model [3]. The advantage of this approach is the possibility of modifying the inelastic versus elastic proportion on scattering events with the energy of the incident electron. So, near electron beam energy of 10 keV, strong variation must occur due to the impossibility of exciting atomic K-levels. Both depth and lateral distributions of generated e–h computed by Monte Carlo algorithms have been compared with recently published experimental measurements [4]. In a second step, the estimated e–h generation function $g(x, y, z)$ is introduced into the steady-state diffusion equation to extract the collection efficiency, i.e., the normalized EBIC at each point of the linescan. This procedure is applied to investigate the total recombination velocity R in separate-confinement laser heterostructures (SCH).

2. Experimental details

The EBIC linescan profiles are collected from SCHs based on InP. These lasers were grown by metal–organic vapour phase epitaxy (MOVPE) on an n-doped (Si: 1×10^{18} cm^{-3}) InP substrate at 900 K and nominal atmospheric pressure (III-V ratio: 100). The heteroepitaxial structure is described schematically in Fig. 1, close to a wedge transmission electron microscopy (WTEM) micrograph of the laser. The undoped active region consists in four InGaAs quantum wells (QWs) of 80 Å width separated by InGaAsP barriers of 170 Å (both InGaAs and InGaAsP are matched to InP). This structure is sandwiched between two InGaAsP layers of 40 nm. This multiple-quantum-well (MQW) is buried below 1.5 μm of a p-doped (Zn: 5×10^{17} cm^{-3}) InP, and 1.0 μm n-doped InP (Si: 3×10^{18} cm^{-3}) was grown between the substrate and the active region. Both layers

* Corresponding author.

PII S0921-5107(96)01701-1

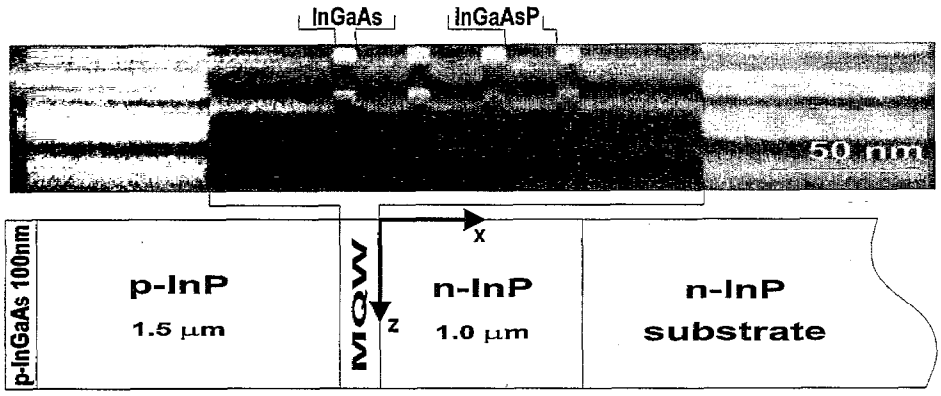

Fig. 1. Scheme of the SCH on study. The WTEM micrograph shows the multiquantum well (MQW) structure.

configure the p–n junction of the SCH. The whole structure is capped by 100 nm of p-doped $In_{0.53}Ga_{0.47}As$ (Zn: 1×10^{19} cm^{-3}).

The EBIC linescans are performed on freshly cleaved (110) face perpendicular to the epilayers in the (001) direction, labelled normal-collector configuration (displayed in Fig. 2). The current induced by electron beam excitation is measured using a Matelect ISM-5A amplifier and Matelect IU-1 interface. The EBIC experimental set-up is installed on a JEOL-820SM scanning electron microscope.

3. Results and discussion

During the high-energy electron brake, e–h are generated while the incident electron energy reaches the energy gap of the semiconductor. To take into account the extent of e–h generation, we have developed a Monte Carlo procedure introducing the s-scattering model as physics frame. In order to calculate EBIC linescans, the number of generated electron-hole pairs $g(\tilde{x}, \tilde{y}, \tilde{z})$ in each scattering event is computed: $g(\tilde{x}, \tilde{y}, \tilde{z}) = [E(i-1) - E(i)]/E_{eh}$, where $E(i)$ is the electron beam energy at the i-step and E_{eh} the energy of an electron–hole pair generation [5].

After its generation, electron–hole pairs diffuse into the semiconductor. At low level injection, the EBIC signal results from the minority carriers that reach the junction. These are swept out to the other side of the space-charge region (SCR) and collected as a current. Therefore, outside the depletion region, the EBIC signal is dominated by the minority carriers diffusion and follows the steady-state equation:

$$D\nabla^2 p(r) - \frac{1}{\tau} p(r) + g(r) = 0, \quad (1)$$

where $g(r)$ is the electron–hole generation at $r(x, y, z)$ coordinates, $p(r)$ is the minority carrier density, D is the diffusion coefficient related to mobility μ by the Einstein relation ($D = \mu \times k_B T/e$) and τ describes the effective minority carrier lifetime that includes the radiative, non-radiative lifetimes and surface recombination process. D and τ are related through minority carriers diffusion length L, $D = L^2/\tau$. The diffusion problem in linescans across p–n junctions may be reduced to two dimensions due to the EBIC and does not depend on the y-coordinate. Therefore, $g(\tilde{x}, \tilde{z})$ and $p(x, z)$ are expressed by the following ($\tilde{x}$, $\tilde{y}$, $\tilde{z}$ are the generation coordinates):

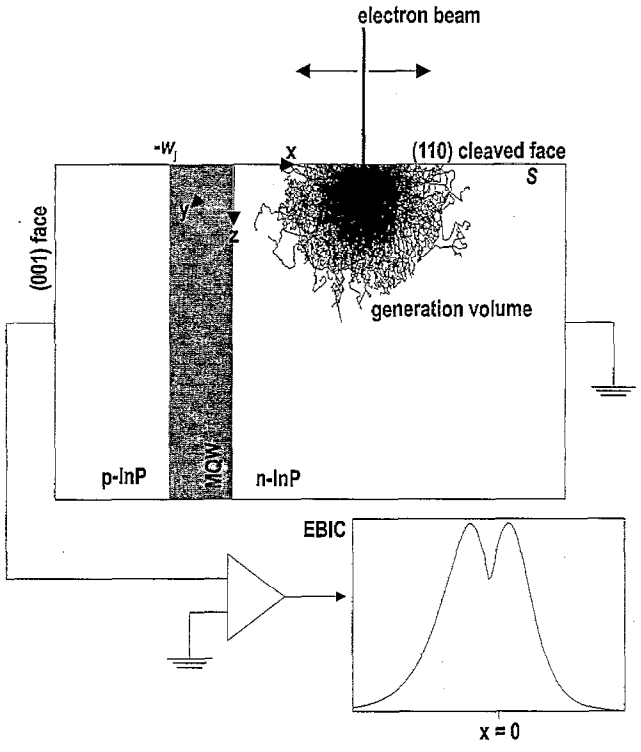

Fig. 2. Geometry used for EBIC profiles measurements, performed along the [001] direction. The generation volume from elastic–inelastic interactions between high-energy beam electrons and the semiconductor is shown. In the scattering model, each interaction generates a quantity of e–h depending on the incident electron energy-loss. Also, the minority carriers collection efficiency depends on coordinates (x, y, z). For example, every e–h generated at MQW recombines.

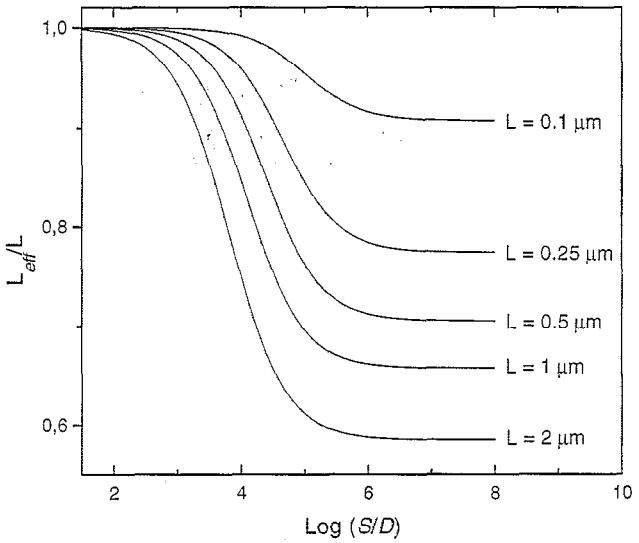

Fig. 3. The L_{eff}/L ratio as a function of S/D for a different bulk minority carriers diffusion lengths L at $E_b = 5$ keV. The effective diffusion length L_{eff} may be evaluated from integrated minority carriers density depth $\bar{z}$ determination, by Monte Carlo integration subroutine (Eqs. (8) and (9)).

$$g(\tilde{x}, \tilde{z}) = \int_{-\infty}^{+\infty} g(\tilde{x}, \tilde{y}, \tilde{z})\, \mathrm{d}y$$

$$p(x, z) = \int_{-\infty}^{+\infty} p(x, y, z)\, \mathrm{d}y. \quad (2)$$

The boundary conditions to solve Eq. (1) are the following. (a) The junction is assumed to be a perfect recombination region for the inside generated e–h, i.e., every e–h generated at MQW recombines. It means that the recombination lifetime in the QWs is shorter than the drift time when the carriers are by pairs. (b) The surface at $z = 0$ (110) is characterized by its recombination velocity S,

$$D\frac{\partial}{\partial z}p(x, z)\bigg|_{z=0} = Sp(x, z)|_{z=0}. \quad (3)$$

(c) Outside the active region, the minority carriers recombination, due to its capture at MQW is, in the same way, characterized by the recombination rate R:

$$D\frac{\partial}{\partial x}p(x, z)\bigg|_{x=-w_j/2} = Rp(x, z)|_{x=-w_j/2}. \quad (4)$$

The collected EBIC profile, $I_{EBIC}(x)$ may be defined as:

$$I_{EBIC}(x) = \int_0^{+\infty} p(x, z)\, \mathrm{d}z = \int_0^{+\infty}\int_0^{+\infty}\int_{-\infty}^{+\infty} g(\tilde{x}, \tilde{z})\varphi(x, z, \tilde{x}, \tilde{z}) \times \mathrm{d}\tilde{x}\, \mathrm{d}\tilde{z}\, \mathrm{d}z, \quad (5)$$

where $\varphi(x, z, \tilde{x}, \tilde{z})$ [6] is the minority carriers collection probability for e–h that are generated at $(\tilde{x}, \tilde{z})$, and collected at (x, z). From Eqs. (3) and (4), the minority carriers density $p(x, z)$, solution of Eq. (1), must be in the form [7]:

$$p(x, z) = p_{3D}(x, z)\left[1 - \frac{\chi}{1+\chi}\exp\left(-\frac{z}{L}\right)\right] \times \left[1 - \frac{\eta}{1+\eta}\exp\left(-\frac{d_j + w_j/2}{L}\right)\right]. \quad (6)$$

We define χ and η as the ratios of minority carriers diffusion length L and the associated depletion lengths D/S and D/R, respectively: $\chi = S \times L/D$ and $\eta = R \times L/D$. The minority carriers density in the absence of surface perturbation (the infinite-3D case) is $p_{3D}(x, z)$:

$$p_{3D}(x, z) = \exp\left(-\frac{d_j}{L_{eff}}\right)\int_0^{+\infty}\int_{-\infty}^{+\infty} g(\tilde{x}, \tilde{z}) \times \exp\left(-\frac{z - \tilde{z}}{L}\right)\mathrm{d}\tilde{x}\, \mathrm{d}\tilde{z}. \quad (7)$$

In the above proposed approximation to p_{3D}, the first exponential term corresponds to lateral (x-axis) dependence on minority carriers density, where d_j and L_{eff} are the distan1ce to the junction's edge (the SCR is located between $-w_j \leqslant x \leqslant 0$) and the minority carriers effective diffusion length, respectively. Hence, $d_j = x$ on the n-side ($x > 0$) and $d_j = -(x + w_j)$ on the p-side ($x < -w_j$). The effective diffusion length is expressed by [8]:

$$L_{eff} = L\sqrt{[1 - \frac{\chi}{1+\chi}\exp(-\frac{\bar{z}}{L})][1 - \frac{\eta}{1+\eta}\exp(-\frac{d_j + w_j/2}{L})]} \quad (8)$$

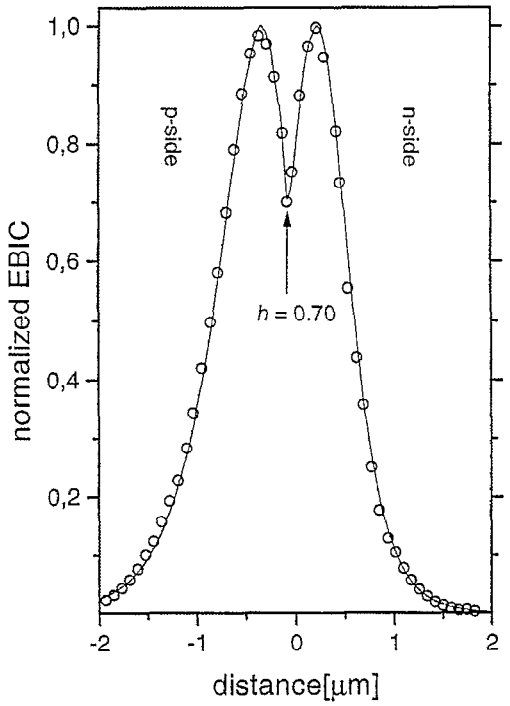

Fig. 4. EBIC-intensity profile across the SCH structure. (○), Experimental data; (——), simulated profile. The distance corresponds to the x-axis of Fig. 2.

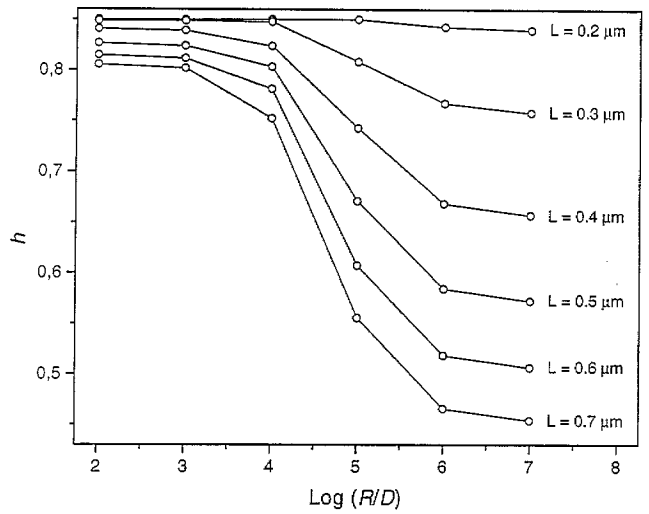

Fig. 5. Minimum minority carriers collection h at MQW vs. R/D ratio for different bulk diffusion length values ($L = 0.2$–0.7 μm).

directly from the assumption $p_{3D}/\tau = p/\tau_{eff}$, where $\bar{z}$, the integrated minority carriers density depth, is expressed as

$$\bar{z} = \frac{1}{\gamma} \int_0^{+\infty} \int_{-\infty}^{+\infty} zp(x, z)\, dx\, dz, \qquad (9)$$

where γ ensures its normalization.

Comparing the calculated EBIC linescans to the experimental measurements, the bulk minority carriers diffusion length L and S/D are deduced. The decrease near the SCR is very sensitive to S/D while the EBIC behaviour far from the junction (> 1.3 μm) is more sensitive to L. Hence, the S/D ratio is close to ∞ in our case ($\log(S/D) \geqslant 6$). We determine the minority carriers effective diffusion lengths by fitting an exponential-like decay on linescans in the region $x > 1$ μm, resulting in $L_{eff} = 0.26$ μm for holes and $L_{eff} = 0.38$ μm for electrons. Fig. 3 displays the dependence of L_{eff}/L on S/D at $E_b = 5$ keV deduced from Eqs. (8) and (9), assuming a large distance from the junction-MQW. From the deduced values of L_{eff}/L and S/D, the bulk diffusion lengths are evaluated to be $L_h = 0.35$ μm at the n-side and $L_e = 0.54$ μm at the p-side.

The experimental normalized-EBIC profile (○) and the closest-fitting simulated profile (——) are shown in Fig. 4. The other feature of these EBIC linescans is the 'hole' in the EBIC intensity due to the carriers capture in the MQW. Indeed, when both electron and hole are present, the recombination lifetime in the QWs becomes shorter than the time to sweep out the carriers of the depletion layer. Obviously, it is not the case when minority carriers reach the junction from both p- and n-sides. Its relative minimum collection amounts to 70% of the maximum. The dependence of the relative hole depth h on the ratio R/D for different bulk diffusion length values is displayed in Fig. 5. As the experimental $h = 0.7$, and knowing L_h and L_e, R/D is found to be $\geqslant 1 \times 10^6$ cm^{-1} and 5×10^4 cm^{-1} for holes (n-side) and electrons (p-side), respectively. However, the recombination rate R must be identical for both electrons and holes. Therefore, mobilities are estimated to be $D_h = 3.25$ cm^2 s^{-1} [9] and $D_e = 65$ cm^2 s^{-1} [10].

In summary, from EBIC measurements, effective diffusion lengths L_{eff} are measured. Introducing these values into the theoretical analytical expressions and comparing them with the experimental shape S/D, R/D, L_e and L_h are deduced. The junction laser characteristics are then $\mu_h = 125$ cm^2 V^{-1} s^{-1}, $\mu_e = 2500$ cm^2 V^{-1} s^{-1} and $R \approx 3 \times 10^6$ cm s^{-1}.

4. Conclusion

A procedure to compute EBIC linescans across QWs is presented. From the extended generation of electron–hole pairs estimated from the Monte Carlo method and applying the steady-state diffusion equation to generated e–h in each differential volume, with the appropriate boundary conditions, the EBIC profile is deduced. From direct comparison between simulated and experimental data, electron and hole mobilities, surface recombination velocity and recombination rate in the active region of the laser are deduced.

Acknowledgements

This work was supported by the CICYT (Comisión Interministerial de Ciencia y Tecnología), under MAT94-0538 Project and by the Junta de Andalucía through Group 6020. The work was carried out at the Electron Microscopy Division of the University of Cádiz. The authors would like to thank J.D. Lambkin of the National Microelectronics Research Centre of Cork (Ireland) for lasers growth.

References

[1] J.-F. Bresse, *Scanning Electron Microsc.*, *4* (1982) 1487.
[2] D.B. Holt, in D.B. Holt and D.C. Joy (eds.), *SEM Microcharacterization of Semiconductors*, Academic Press, London, 1989.
[3] M.J. Romero, D. Araújo and R. García, *Mat. Sci. Eng.*, *B42* (1996) 168.
[4] J.-M. Bonard, J.-D. Ganière, B. Akamatsu and D. Araújo, *J. Appl. Phys.*, *79* (1996) 8693.
[5] H.J. Leamy, *J. Appl. Phys.*, *53* (1982) R51.
[6] C. Donolato, *Inst. Phys. Conf. Ser.*, *100* (1989) 715.
[7] M. Watanabe, G. Actor and H.C. Gatos, *IEEE Trans. Electron Devices*, *24* (1977) 1172.
[8] L. Jastrzebski, J. Lagowski and H.C. Gatos, *Appl. Phys. Lett.*, *27* (1975) 537.
[9] E. Kubota, Y. Ohmori and K. Sugii, *J. Appl. Phys.*, *55* (1984) 3779.
[10] Y. Takeda and A. Sasaki, *Solid-State Electron.*, *27* (1980) 2659.